A&A 568, A2 (2014)
DOI: 10.1051/0004-6361/201424135

Astronomy & Astrophysics

The *Gaia*-ESO Survey: Metallicity of the Chamaeleon I star-forming region⋆,⋆⋆

L. Spina[1], S. Randich[1], F. Palla[1], K. Biazzo[2], G. G. Sacco[1], E. J. Alfaro[3], E. Franciosini[1], L. Magrini[1], L. Morbidelli[1], A. Frasca[2], V. Adibekyan[4], E. Delgado-Mena[4], S. G. Sousa[4,5], J. I. González Hernández[6,7], D. Montes[8], H. Tabernero[8], G. Tautvaišienė[9], R. Bonito[10], A. C. Lanzafame[11], G. Gilmore[12], R. D. Jeffries[13], A. Vallenari[14], T. Bensby[15], A. Bragaglia[16], E. Flaccomio[10], A. J. Korn[17], E. Pancino[16,18], A. Recio-Blanco[19], R. Smiljanic[20], M. Bergemann[12], M. T. Costado[3], F. Damiani[10], V. Hill[19], A. Hourihane[12], P. Jofré[12], P. de Laverny[19], C. Lardo[16], T. Masseron[12], L. Prisinzano[10], and C. C. Worley[12]

[1] INAF – Osservatorio Astrofisico di Arcetri, Largo E. Fermi 5, 50125 Firenze, Italy
e-mail: lspina@arcetri.astro.it
[2] INAF – Osservatorio Astrofisico di Catania, via S. Sofia, 78, 95123 Catania, Italy
[3] Instituto de Astrofísica de Andalucía-CSIC, Apdo. 3004, 18080 Granada, Spain
[4] Centro de Astrofisica, Universidade do Porto, rua das Estrelas, 4150-762 Porto, Portugal
[5] Departamento de Física e Astronomia, Faculdade de Ciências, Universidade do Porto, rua do Campo Alegre, 4169-007 Porto, Portugal
[6] Instituto de Astrofisica de Canarias (IAC), 38205 La Laguna, Tenerife, Spain
[7] Depto. Astrofisica, Universidad de La Laguna (ULL), 38206 La Laguna, Tenerife, Spain
[8] Departamento de Astrofisica, Universidad Complutense de Madrid (UCM), Spain
[9] Institute of Theoretical Physics and Astronomy, Vilnius University, Gostauto 12, LT-01108 Vilnius, Lithuania
[10] INAF – Osservatorio Astronomico di Palermo, Piazza del Parlamento 1, 90134 Palermo, Italy
[11] Dipartimento di Fisica e Astronomia, Sezione Astrofisica, Università di Catania, via S. Sofia 78, 95123 Catania, Italy
[12] Institute of Astronomy, University of Cambridge, Madingley Road, Cambridge CB3 0HA, UK
[13] Astrophysics Group, Research Institute for the Environment, Physical Sciences and Applied Mathematics, Keele University, Keele, Staffordshire ST5 5BG, UK
[14] INAF – Padova Observatory, Vicolo dell'Osservatorio 5, 35122 Padova, Italy
[15] Lund Observatory, Department of Astronomy and Theoretical Physics, Box 43, 221 00 Lund, Sweden
[16] INAF – Osservatorio Astronomico di Bologna, via Ranzani 1, 40127 Bologna, Italy
[17] Department of Physics and Astronomy, Uppsala University, Box 516, 75120 Uppsala, Sweden
[18] ASI Science Data Center, via del Politecnico SNC, 00133 Roma, Italy
[19] Laboratoire Lagrange (UMR7293), Université de Nice Sophia Antipolis, CNRS, Observatoire de la Côte d'Azur, CS 34229, 06304 Nice Cedex 4, France
[20] Department for Astrophysics, Nicolaus Copernicus Astronomical Center, ul. Rabiańska 8, 87-100 Toruń, Poland

Received 5 May 2014 / Accepted 8 June 2014

ABSTRACT

Context. Recent metallicity determinations in young open clusters and star-forming regions suggest that the latter may be characterized by a slightly lower metallicity than the Sun and older clusters in the solar vicinity. However, these results are based on small statistics and inhomogeneous analyses. The *Gaia*-ESO Survey is observing and homogeneously analyzing large samples of stars in several young clusters and star-forming regions, hence allowing us to further investigate this issue.
Aims. We present a new metallicity determination of the Chamaeleon I star-forming region, based on the products distributed in the first internal release of the *Gaia*-ESO Survey.
Methods. The 48 candidate members of Chamaeleon I have been observed with the high-resolution, spectrograph UVES. We use the surface gravity, lithium line equivalent width, and position in the Hertzsprung-Russell diagram to confirm the cluster members, and we use the iron abundance to derive the mean metallicity of the region.
Results. Out of the 48 targets, we confirm 15 high probability members. Considering the metallicity measurements for nine of them, we find that the iron abundance of Chamaeleon I is slightly subsolar with a mean value [Fe/H] = −0.08 ± 0.04 dex. This result agrees with the metallicity determination of other nearby star-forming regions and suggests that the chemical pattern of the youngest stars in the solar neighborhood is indeed more metal-poor than the Sun. We argue that this evidence may be related to the chemical distribution of the Gould Belt that contains most of the nearby star-forming regions and young clusters.

Key words. open clusters and associations: individual: Chamaeleon I – stars: pre-main sequence – stars: abundances – techniques: spectroscopic

⋆ Based on observations collected at the ESO telescopes under programme 188.B3002, the *Gaia*-ESO large public spectroscopic survey.
⋆⋆ Tables 1–3 are available in electronic form at http://www.aanda.org

1. Introduction

The metallicity determination in young open clusters (YOCs) and star-forming regions (SFRs) has implications for fundamental topics, such as the origin and early evolution of these environments, the evolution of circumstellar disks, and the ability to form planets (see Gilli et al. 2006; Neves et al. 2009; Ercolano & Clarke 2010; Yasui et al. 2010; Kang et al. 2011; Spezzi et al. 2012; Adibekyan et al. 2012a,b; Spina et al. 2014, and references therein). Furthermore, these young regions are of particular interest, since they are still close to their birthplace and contain a homogeneous stellar population that had no time to disperse through the Galactic disk. Thus, YOCs and SFRs are key objects to trace the present chemical pattern of the Galactic thin disk. Indeed, an increasing number of studies has focused on the metallicity of YOCs and SFRs in the last few years (e.g., James et al. 2006; González Hernández et al. 2008; Santos et al. 2008; D'Orazi & Randich 2009; D'Orazi et al. 2009, 2011; Viana Almeida et al. 2009; Biazzo et al. 2011a,b, 2012a,b; Spina et al. 2014). These studies suggest that YOCs, where star formation has ceased, generally share a metallicity close to the solar value; on the other hand, SFRs, in which the molecular gas is still present and the star formation process is still ongoing, surprisingly seem to be characterized by a somewhat lower iron content. The question arises whether this result is due to low-number statistics and/or to inhomogeneous methods that derive the metallicity or that the metallicity determination in very young stars in SFRs is more uncertain and generally based on rather cool stars. On the other hand, if confirmed, this result would have important implications for our understanding of the origin of YOCs and SFRs.

The *Gaia*-ESO Survey (Gilmore et al. 2012; Randich & Gilmore 2013) is currently observing a significant number of young environments. While the main goal of the young cluster observations is the study of their kinematics and dynamical evolution through the measurement of accurate radial velocities (e.g., Jeffries et al. 2014), this large amount of data can also be used to perform a homogeneous study of the elemental abundances of YOCs and SFRs. In this framework, we have determined the metal content of Gamma Velorum in a recent study, which is the first YOC observed by the *Gaia*-ESO Survey (Spina et al. 2014). The present paper is devoted to the analysis of the metallicity of the first SFR targeted by the *Gaia*-ESO Survey: Chamaeleon I (hereafter, Cha I). A detailed analysis of the membership and other properties of the cluster, which is mostly based on the GIRAFFE data, will be reported in Sacco et al. (in prep.).

With a mean age of ∼2 Myr (Luhman 2007) and its proximity to the Sun (d = 160−165 pc; Whittet et al. 1997), Cha I is one of the best studied SFRs. It is part of a wider star-forming complex, which is distributed over a region of a few square degrees, that contains also two smaller molecular clouds, Cha II and Cha III (Schwartz 1977). Cha I has been the target of many spectroscopic and photometric surveys that have uncovered a large population of embedded and optically visible sources (see the review by Luhman 2008; hereafter, L08). The current sample of known members comprises 237 sources (hereafter, "L08-mem"), extending down to substellar objects. The census is nearly complete in the central regions of Cha I ($11^\circ05' \leq$ RA $\leq 11^\circ11'$; $-77^\circ48' \leq$ Dec $\leq -76^\circ18'$) for $M \geq 0.03\ M_\odot$ and $A_J \leq 1.2$, but the stellar population outside this area is still not completely identified (Luhman 2007). Recently, López Martí et al. (2013) have identified 51 new kinematical candidate members that await confirmation through accurate spectroscopic data. The initial mass function (IMF) of Cha I has been explored down to substellar masses by Luhman (2007) and, as with other SFRs, it reaches a maximum between 0.1 and 0.2 $M_\odot$. L08, using *Spitzer* colors to study the disk population, argued that the lifetimes of disks around solar-mass stars are longer in Cha I than in other young clusters, probably because of the lower stellar density and resulting reduction in dynamical interactions. On the other hand, Cha I is also characterized by a number of subsolar-mass stars with unusually short disk lifetimes (Luhman 2007; Robberto et al. 2012). The Cha I association can be distinguished in two sub-clusters, Cha I North (Dec $> -77^\circ$) and Cha I South (Dec $< -77^\circ$), with different star formation histories. The distribution of isochronal ages suggests that star formation began ∼5−6 Myr ago in the northern portion and developed later in the southern extension (Luhman 2007).

Cha I is relatively isolated from other SFRs and does not contain numerous massive stars. Two metallicity determinations have been already published prior to our study: in the first one, Padgett (1996) derived an average value of $\langle$[Fe/H]$\rangle = -0.07 \pm 0.06$ dex; a subsequent study by Santos et al. (2008) reports $\langle$[Fe/H]$\rangle = -0.11 \pm 0.14$, but this estimate is based on the analysis of four stars that are located in a wide area of the Chamaeleon complex, which is away from the main SFRs. Furthermore, in a recent work on proper motions, López Martí et al. (2013) have shown that two of these four stars, namely RX J1158.5−7754a and RX J1159.7−7601, seem to be kinematical members of the ϵ Cha association; another (RX J1140.3−8321) is of the η Cha association, while RX J1233.5−7523 is a field star. Thus, the metallicity of Santos et al. (2008) is not representative of the SFR, and a new dedicated study is both necessary and timely.

The paper is organized as follows: in Sect. 2, we describe the target selection and spectral analysis. The identification of the cluster members are on the basis of the surface gravity, the detection of lithium in the stellar atmospheres and their position in the Hertzsprung-Russell diagram is presented in Sect. 3. The results of the elemental abundance determination are discussed in Sect. 4. In Sect. 5, we overview and discuss the metal content of SFRs in a broader context. Sect. 6 summarizes our findings.

2. *Gaia*-ESO data

The analysis presented in this paper is based on the spectroscopic data obtained by the *Gaia*-ESO Survey during the first six months of observations (January−June 2012) and following the analysis released internally to the survey consortium in the iDR1 catalog at the Wide Field Astronomy Unit at Edinburgh University[1]. In this section, we describe the target selection, the observations, and the available data products of the *Gaia*-ESO Survey analysis.

2.1. Target selection and observations

The *Gaia*-ESO Survey observations are performed with the multi-object optical spectrograph FLAMES at the VLT (Pasquini et al. 2002) using both GIRAFFE and UVES. In this paper, we focus on the latter, while GIRAFFE targets and their properties will be discussed in a forthcoming paper by Sacco et al. (in prep.).

The selection criteria are based on homogeneous photometric data, covering a large area of the cluster field, following the *Gaia*-ESO Survey guidelines for cluster observations (see Bragaglia et al. 2014). The UVES targets have been selected

[1] The GESviDR1Final catalog at http://ges.roe.ac.uk/

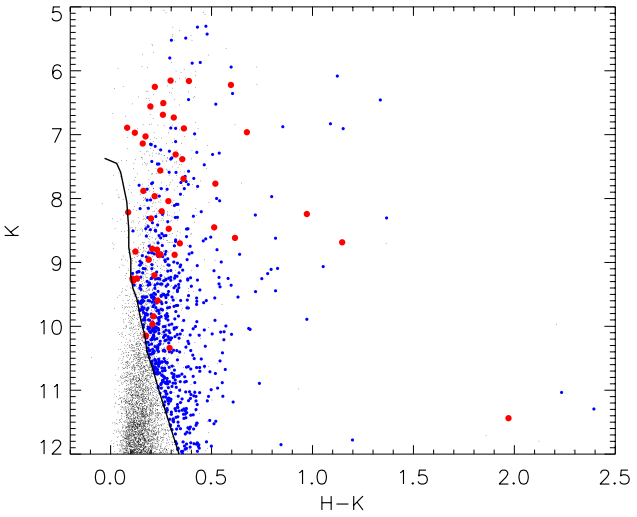

Fig. 1. Infrared color−magnitude diagram for the stars lying in the cluster field and having $R_{\rm USNO} \leq 17.0$. The black line represents the 10 Myr isochrone using Siess et al. (2000) models. Blue (small) and red (large) dots are the stars targeted with GIRAFFE and UVES, respectively.

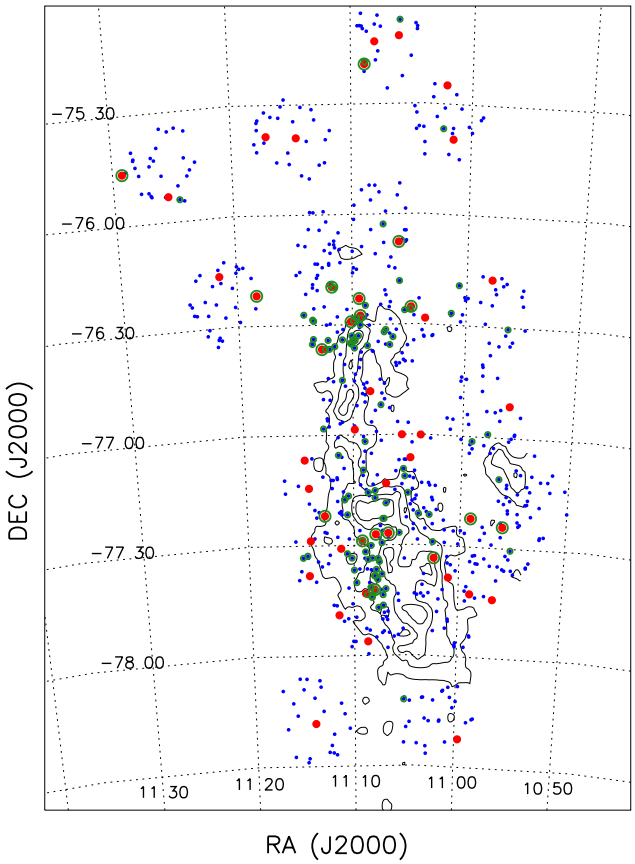

Fig. 2. Map of the observed sources in the Cha I fields. Blue (small) dots are the GIRAFFE targets, and red (large) dots are the UVES ones. Green circles mark the "L08-mem". The contours correspond to the extinction map of Cambresy (1998) at inside-out intervals of A_V = 8, 6, 4, and 2 mag.

by including only those sources that i) are located in the central and most populated area of the cluster but wide enough to extend into the cluster boundaries (i.e.,10°45′ ≤ RA ≤ 11°30′; −79°00′ ≤ Dec ≤ −75°00′); ii) have $R_{\rm USNO}$[2] ≤ 17.0; iii) have avaliable 2MASS photometry (Cutri et al. 2003); iv) fall above the 10 Myr isochrone in the K vs. $H-K$ diagram, as shown in Fig. 1 using the Siess et al. (2000) models. For the UVES targets, high priority was given to stars already identified as members by L08 with the spectral type that is earlier than ∼$M0$. However, several other sources were actually observed for a best exploitation of the available fibers.

A total of 25 fields covering the regions of Cha I, as shown in Fig. 2, were observed in runs C, D, and E (March−May, 2012), using the UVES/CD#3 cross disperser (λ = 4770−6820 Å; R = 47 000). Seventeen fields have been chosen to cover the central region of the cluster (hereafter, on-fields), as characterized by a higher extinction and rich in confirmed members. To obtain a complete sampling of the members and possibly discover other candidates missed in previous studies, eight additional fields (off-fields) have been placed in the northern and southern periphery of the association to observe its sparse population. Sixteen and nine OBs were observed for 20 ($R_{\rm USNO}$ between 12 and 14 mag) and 50 min ($R_{\rm USNO}$ between 14 and 17 mag), respectively. Eleven of the stars have a longer exposure time because of the partial overlap of the fields.

A total of 48 UVES spectra were acquired. The sample includes only 18 L08 members, as most of the 237 members are M-type stars (and were thus observed with GIRAFFE) or brown dwarfs that are fainter than the survey limit. One of the kinematic candidate members, 2MASS J10593816−7822421, identified by López Martí et al. (2013) has also been observed. The signal-to-noise ratio (S/N) of the spectra is in the range 5−300 with a median value ∼60. The 48 targets are listed in Table 2, where we include a running ID, the CNAME, coordinates (J2000), S/N, J magnitude, and the membership flag from L08 ("Y" for members and "–" for the stellar object with an unassessed membership from Luhman's papers) and a multiplicity flag.

[2] USNO-A2.0 (Monet et al. 2008) is a catalog of 526,280,881 stars that lists right ascension and declination (J2000) and the standard Landolt B and R magnitude for each star.

2.2. Available data from the Gaia-ESO Survey

As mentioned above, we use the products released in the iDR1 catalog for the Cha I region, which consist of radial velocities, projected rotational velocities, spectroscopic cross-correlation functions (CCFs), fundamental stellar parameters ($T_{\rm eff}$, log g, [Fe/H]), equivalent width of the Li line at 6708 Å, and Hα with an uncertainty for each quantity. The UVES data are reduced using the FLAMES-UVES ESO public pipeline. The determination of radial and rotational velocities is described in detail in Sacco et al. (2014). A specific working group of the *Gaia*-ESO consortium is dedicated to the analysis of cool young stars. For UVES spectra, this working group benefits the contribution of four nodes that use different methods of analysis, which can be summarized as follows: i) the equivalent width (EW) analysis, where the atmospheric parameter determination is based on the excitation and ionization balance of the iron lines; ii) spectral classification and estimated atmospheric parameters from a χ^2 fit of the observed spectra with a grid of templates that are composed by observed spectra of slow-rotating, low-activity stars. The parameters released in iDR1 catalog are obtained by computing the median value of the results provided by the nodes after the outliers have been discarded. Uncertainties are the node-to-node dispersions. We mention that all the working groups of the consortium devoted to the spectroscopic analysis of F-, G-, K-, and M-type stars uniformly makes use of MARCS models of stellar atmospheres (Gustafsson et al. 2008), which assume the solar abundances from Grevesse et al. (2007). Common atomic

data have also been used for the analysis of all the spectra of the *Gaia*-ESO Survey (Heiter et al. 2014). Similarly, more than one node measures the strength of the Li I line at 6707.8 Å in both Giraffe and UVES spectra. They use independent methods to derive the EW of this features: specifically, some of them apply a Gaussian fitting to the line, while others are based on the direct profile integration of the line. The median value of the EW (or the average, when only two nodes provided the measurement) corrected for the spectral veiling are then adoped. All these procedures are detailed in Lanzafame et al. (in prep.).

The available products for the 48 targets are listed in Table 3, where we report the following quantities: running number, radial velocity, rotational velocities, fundamental parameters, equivalent width of the Li line, the estimate of the bolometric luminosity ($L_{\rm bol}$), and the information on binarity and membership resulting from our analysis (see Sect. 3). The $L_{\rm bol}$ values have been derived from the $J_{\rm 2MASS}$ magnitudes corrected for the extinction and assume the distance of the cluster as 160 pc, as previously determined by Whittet et al. (1997). Namely, the extinction has been estimated from the difference between the photometric and spectroscopic temperatures, while photometric temperatures and bolometric corrections have been derived by adopting the calibrations of Pecaut & Mamajek (2013). The $L_{\rm bol}$ errors take the uncertainties on the magnitudes, spectroscopic temperatures, and cluster distance into account. The mean uncertainties on the stellar parameters are $\langle\sigma_{T_{\rm eff}}\rangle$ = 126 K, $\langle\sigma_{\log\ g}\rangle$ = 0.25 dex, and $\langle\sigma_{\rm [Fe/H]}\rangle$ = 0.13 dex.

As indicated in the table, the values of the main parameters have been derived for 42 of the initial 48 UVES targets. The remaining stars could not be analyzed due to the poor S/N or because of the presence of strong spectral veiling. Radial velocities are available for 42 targets. Sixteen out of 42 are L08 members. Since the main aim of this paper is to determine the metal content of Cha I, we consider only those stars with the main parameters available in the following.

3. Membership analysis of UVES targets

We have identified two double-lined binaries (SB2) through the spectral CCFs: #22 and #27 in Table 3. Their binarity was known also from previous studies (i.e., Covino et al. 1997; Lafrenière et al. 2008). We do not consider these systems for membership analysis, even though the *Gaia*-ESO Survey provides the stellar parameters for one of them, because the determination is likely to be unreliable.

Following the same procedure adopted in Spina et al. (2014) for the Gamma Velorum cluster, we use the spectroscopic information and the position of the stars in the Hertzsprung-Russell diagram (HRD) to carry out the membership analysis in this Section. This is performed on the 41 UVES targets, whose main parameters have been determined by the *Gaia*-ESO consortium, and that have not been flagged as SB2. This sample contains 15 "L08 mem".

3.1. Identification of the giant contaminants

The sequence of Cha I members is not clearly identifiable in the CMD of Fig. 1, since the sample of targets is contaminated by field stars. To discard the population of evolved contaminants, we consider for further analysis only those stars with a spectroscopic log $g \gtrsim 3.5$ dex, since stars with lower values of surface gravities are likely background giants. Among the 41 stars with log g determinations, 20 have been rejected as evolved contaminants and, as expected, none of them is a "L08-mem". On the other hand, all the remaining 21 targets are flagged as candidate members, and their membership has been assessed using the lithium equivalent width, as shown below.

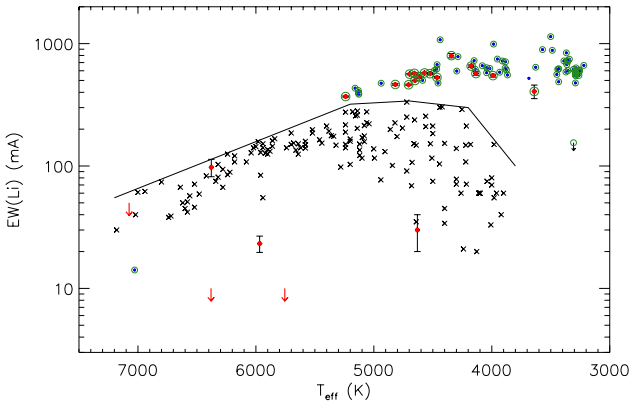

Fig. 3. Lithium EW as a function of the $T_{\rm eff}$ for the candidate members of Cha I. The red (large) dots identify the UVES stars. Most of the Li detections in UVES spectra have uncertainties associated to their EWs smaller than the data points. The GIRAFFE members identified by Sacco et al. (in prep.) with a $T_{\rm eff}$ determination are shown by the smaller blue dots. All the "L08-mem" are marked with a green circle. The solid line denotes the upper-envelope of the Pleiades distribution (crosses; Soderblom et al. 1993; Jones et al. 1996).

3.2. Lithium members

In Fig. 3, we show the EWs as a function of $T_{\rm eff}$ for the 21 UVES sources that have not been rejected as SB2 or giant contaminants. To identify the sequence of cluster members, we also plot the GIRAFFE targets confirmed as cluster members by Sacco et al. (in prep.) on the basis of the equivalent width of the Li line at 6078 Å and the Hα width at the 10% of the peak. For these stars, they list the EWs(Li) and main parameters recommended by the *Gaia*-ESO Survey, which are the values plotted in Fig. 3.

The distribution of "L08-mem", of which most are cooler than ~5300 K and have a EW(Li) > 300 mÅ, clearly defines the sequence of Li undepleted members. To assess the membership of the UVES sources on the basis of the lithium content, we also use the available information for the members of the Pleiades cluster (~125−130 Myr; Stauffer et al. 1998), which is similar to the approach of Spina et al. (2014). The comparison of the EWs(Li) of our stars with those of Pleiades members with similar $T_{\rm eff}$ allows us to identify the youngest targets, which are likely members of Cha I. Among the UVES targets, 15 stars have EW(Li) higher than their Pleiades counterparts, since they lie above the upper-envelope of the Pleiades Li-temperature distribution. Not surprisingly, all these stars, hereafter flagged as Li-members, have EW(Li) > 300 mÅ and are "L08-mem". In contrast, four UVES targets have EW(Li) ≤ 30 mÅ and are located significantly below the Pleiades distribution. The latter are likely field contaminants. Two additional objects that are warmer than 6000 K at $T_{\rm eff}$ = 6378 K and 7075 K lie slightly below the upper-envelope of the Pleiades and have lithium EWs, which are compatible with a pre-main-sequence cluster. However, since Li is no longer a good age tracer for such stars, we consider them as "hot-candidate-members" (HCMs) and try to derive their association with Cha I from the position in the HRD.

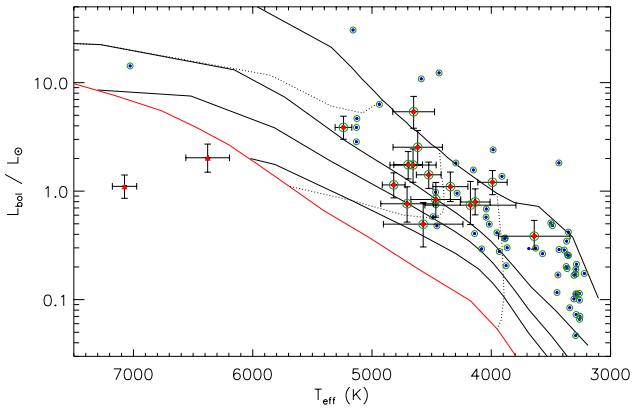

Fig. 4. HR diagram of the UVES Li-members (red large dots), and HCMs (red triangles). All the "L08 mem" are marked with a green circle. The members targeted by GIRAFFE are shown as small blue dots. The dotted and solid black lines are the evolutionary tracks for 0.5, 1, and 2 $M_\odot$ and isochrones for 1, 5, 10, and 20 Myr, respectively. The ZAMS is marked with a solid red line. The evolutionary tracks, the isochrones and the ZAMS are from the stellar models of Siess et al. (2000) for a chemical composition with $Z = 0.01$.

3.3. Hertzsprung-Russell diagram

The HRD can be used to test the reliability of our membership analysis and to provide some additional information about the HCMs for which we were not able to establish a secure membership based on lithium. Using the bolometric luminosity and the effective temperature from the *Gaia*-ESO Survey, we plot the UVES Li-members and the HCMs in the HRD of Fig. 4 with the GIRAFFE members identified by Sacco et al. (in prep.). As for the $T_{\rm eff}$, the $L_{\rm bol}$ values adopted for the GIRAFFE targets are those listed by Sacco et al. (in prep.) and derived with the same procedure used in the present paper for the UVES targets. Overlaid on the data are the 1, 5, 10, and 20 Myr isochrones, the zero-age-main-sequence (ZAMS), and the evolutionary tracks for stars with 0.5, 1, and 2 $M_\odot$ from Siess et al. (2000) models for a stellar metallicity of $Z = 0.01$. The great majority of the Li-members ($T_{\rm eff} < 5500$ K) occupy a region of the diagram between the 1 and 5 Myr isochrones, which agree with the cluster mean age of ~2 Myr that is estimated by Luhman (2007). On the other hand, both HCMs are considerably below the ZAMS and one of them has a radial velocity inconsistent with the mean RV for Cha I reported by Sacco et al. (in prep.) ($\langle {\rm RV} \rangle = 14.85 \pm 0.018$ and $\sigma_{\rm RV} = 1.1 \pm 0.16$ km s^{-1}), suggesting that they are likely contaminants. Therefore, we reject them from further analysis.

3.4. Conclusion on the membership analysis

The membership flags for each of the UVES stars derived from log g, lithium EWs and HRD are summarized in Table 3. In total, there are 15 secure members that satisfy our membership criteria. Since all these stars have been previously defined as Cha I members by L08, there is no new member among the UVES targets. Conversely, all the L08 with *Gaia*-ESO parameters are confirmed as members. Finally, we have also found that the kinematic candidate member #7 identified by López Martí et al. (2013) have a photospheric lithium and a surface gravity incompatible for a pre-main–sequence star; thus, it is a likely contaminant.

In Fig. 5, we show the spatial distribution of the 15 UVES and 103 GIRAFFE members for the Cha I cloud. We use this information to check if a difference in metallicity is present between the northern and southern sub-clusters and the distributed population.

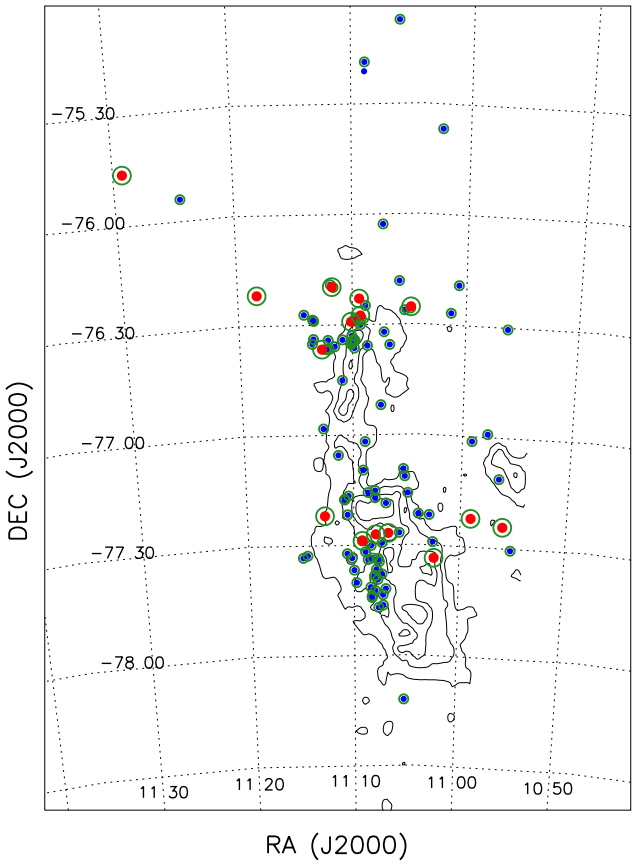

Fig. 5. Map of the spatial location of the Cha I members. The symbols are the same as in Fig. 4. The contours correspond to the extinction map of Cambresy (1998) at inside-out intervals of $A_V = 8$, 6, 4, and 2 mag.

4. The metallicity of Cha I

Based on the 15 UVES members, we derive the [Fe/H] distribution of Cha I shown in Fig. 6. The weighted mean of the distribution is $\langle {\rm [Fe/H]} \rangle = -0.10 \pm 0.04$ dex. We note that the error of the mean (0.04 dex) is small compared to the width of the distribution that extends from −0.45 to 0.00 dex and to the standard deviation $\sigma_{\rm [Fe/H]} = 0.13$ dex that is computed without assigning any weight. We believe that the large excursion of [Fe/H] values is due to the lower accuracy of the more discrepant values rather than to a real dispersion. In support of this claim, we observe that the two most-metal poor stars (#28 and 32) are also those with the biggest errors. Furthermore, we highlight the results for different regions of the cluster with different colors in Fig. 6: Cha I North, Cha I South, and the sparse population. We see that there is no spatial segregation of the iron content in the cluster which is characterized by a homogeneous distribution.

Interestingly, six UVES members have been identified by Lafrenière et al. (2008) as part of tight[3] multiple systems (see Col. 5 in Table 2), namely #21, 28, 29, 32, 36, and 45. Although we do not infer any evidence of binarity from their spectra, we obtain the distribution shown in Fig 7 if we exclude their [Fe/H] values. In this case, the resulting weighted mean is

[3] Since the UVES fiber has a diameter of 1″, we consider "tight systems" only those with a separation ≤2″.

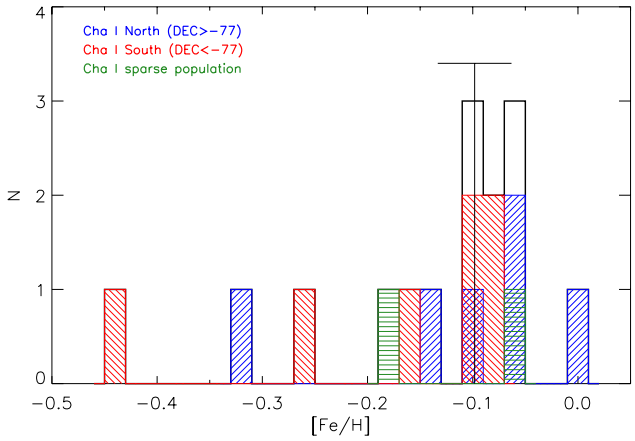

Fig. 6. Iron abundance distribution of the 15 UVES members. The resulting weighted mean metallicity of Cha I is $\langle$[Fe/H]$\rangle$ = −0.10 ± 0.04 dex. The different colors highlight the contribution of the different populations of the cluster, Cha I North, South, and the sparse population.

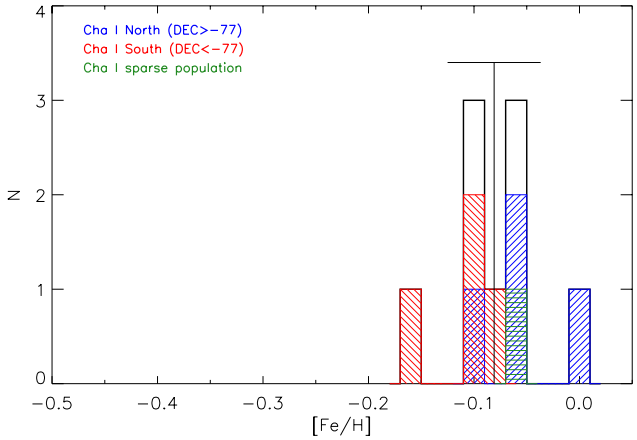

Fig. 7. Iron abundance of the nine UVES members that have not been identified as tight binaries by Lafrenière et al. (2008). The resulting weighted mean metallicity of Cha I is $\langle$[Fe/H]$\rangle$ = −0.08 ± 0.04 dex. Colors are the same of Fig. 6.

similar to the previous one, $\langle$[Fe/H]$\rangle$ = −0.08 dex, but with a significantly lower standard deviation $\sigma_{[Fe/H]}$ = 0.04 dex. We consider this mean as the final metallicity value of Cha I and take its error as the standard deviation around the mean: [Fe/H] = −0.08 ± 0.04 dex.

As a check to asses the reliability of the iron abundances produced by the *Gaia*-ESO Survey, we show [Fe/H] as a function of the effective temperature for the nine stars that have been used to derive the mean cluster metallicity in Fig. 8. For comparison, we also include the results obtained in Gamma Velorum within the *Gaia*-ESO Survey. Clearly, no trend with temperature is visible across the temperature range ∼3500−6500 K, indicating that no bias is affecting our analysis even at the lowest temperatures.

5. Discussion

5.1. Comparison with a previous metallicity determination of CS Cha

As described in Sect. 4, our iron abundance analysis is based on a sample of nine stars observed with UVES. Of these, only one (namely, CS Cha; #11 in Table 2) had been previously observed

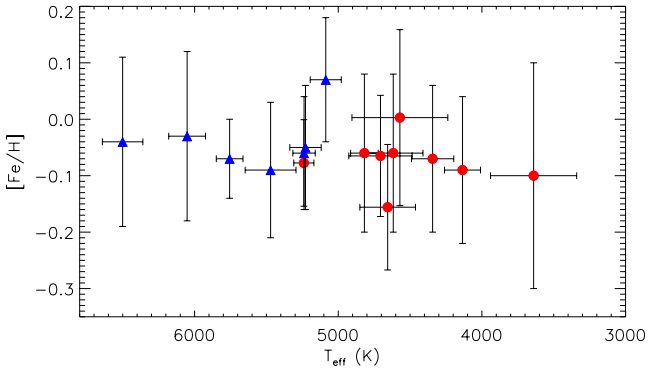

Fig. 8. Iron abundance as a function of $T_{\rm eff}$ for the nine Cha I members (red circles) and the seven stars classified as members of Gamma Velorum by Spina et al. (2014).

and analyzed to derive the iron abundance by Padgett (1996). The *Gaia*-ESO value for this star is [Fe/H] = −0.16 ± 0.11 dex, which is very different from that [Fe/H] = +0.11 ± 0.14 dex quoted by Padgett (1996). We believe that the difference occurs because the analysis by Padgett was based on few iron lines (16) compared to the ∼100−200 lines generally used in the *Gaia*-ESO Survey analysis. Moreover, strong lines that are heavily affected by the treatment of damping were not excluded in Padgett's list. In the case of CS Cha, five of the 16 lines used for the iron abundances have $EW > 150$ mÅ. As a consequence, the micro-turbulent velocity found by Padgett (1996), $\xi = 0.3 \pm 0.6$ km s^{-1}, is much lower than the mean value of $\xi \sim 1.7$ km s^{-1} obtained for the other four stars and the similar value found for other young stars by, e.g., Biazzo et al. (2011a). Low values of ξ can lead to a large overestimation of the iron abundance. Indeed, the CS Cha is the star with the highest iron abundance, [Fe/H] = +0.11 dex, while the other values found by Padgett vary between −0.26 and 0.00 dex.

5.2. Iron abundance in the Chamaeleon complex

We now discuss the overall metallicity of the Chamaeleon complex. In Fig. 9, our [Fe/H] determination for Cha I is compared with previous estimates by Padgett (1996) and Biazzo et al. (2012a). Padgett analyzed five stars associated with the Cha I dark cloud, while Biazzo et al. (2012a) analyzed only one target in Cha II, namely Hn 23. Our estimate of the average metallicity of Cha I ([Fe/H] = −0.08 ± 0.04) is in good agreement within the error bars with the results by Padgett (1996), who derived a mean value of [Fe/H] = −0.06 ± 0.14[4].

It is also clear from Fig. 9 that our [Fe/H] distribution is narrower than that obtained by Padgett (1996) (−0.26 to +0.11 dex) and that the star-to-star variation in metallicity is smaller than the observational errors. Unlike Padgett's conclusion that the dispersion of [Fe/H] in Cha I is larger than that of older clusters, our analysis shows that this is not the case. We believe that Padgett's results can be attributed to the uncertainties that affect the abundance analysis of young stars (e.g., low quality spectra, uncertain stellar parameters, and high activity level, etc.) and not to a real dispersion in metallicity of a given SFR. Indeed, homogeneous abundance measurements have been found in other SFRs, such as the sub-groups of the Orion complex reported by

[4] For consistency, we report the weighted mean of [Fe/H] as the average value of the iron abundance, while the error is the standard deviation around the mean. This determination includes the iron abundance of CS Cha.

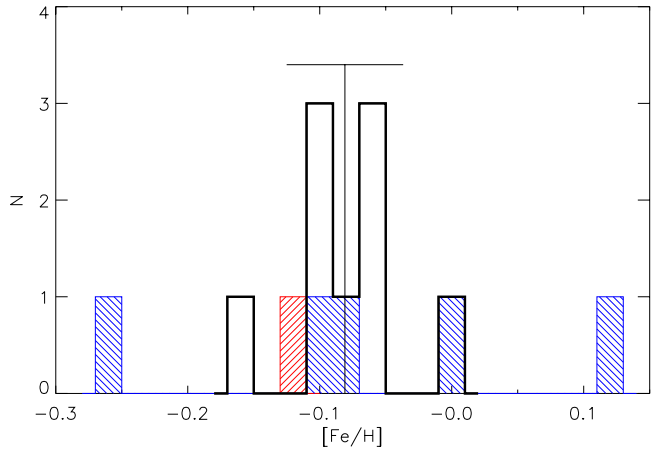

Fig. 9. Comparison between our [Fe/H] distribution (black histogram) with previous estimates by Padgett (1996) (blue histogram) and the single value by Biazzo et al. (2012a) for Cha II (in red). The mean [Fe/H] for the Cha I members and its standard deviation derived in this paper are also indicated by the solid line.

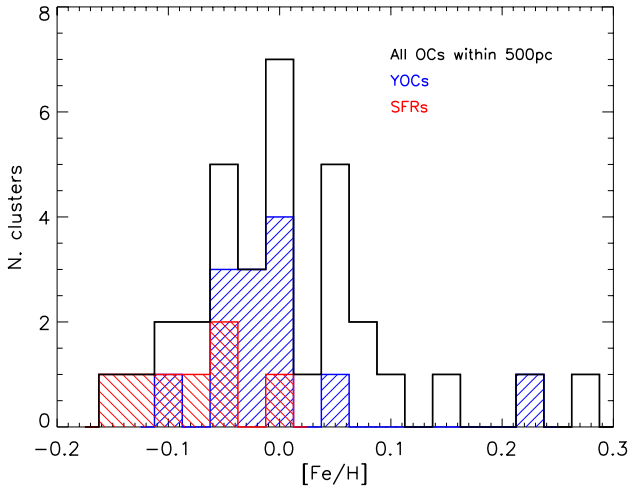

Fig. 10. [Fe/H] distribution of the open clusters and SFRs in the solar neighborhood within a distance of 500 pc. Adopted ages, distances, and metallicity values are listed in Table 1. The red and blue colors denote the SFRs and YOCs subsamples, respectively.

González Hernández et al. (2008), D'Orazi et al. (2009), Biazzo et al. (2011a,b) and the Taurus-Auriga association analyzed by D'Orazi et al. (2011).

Furthermore, we note that the iron abundance [Fe/H] = −0.12 ± 0.14 found in Cha II by Biazzo et al. (2012a) from the analysis of the UVES spectrum of Hn 23 strengthens our conclusion for a subsolar metallicity of the Chamaeleon complex. To test the consistency of the *Gaia*-ESO results with those of Biazzo et al. (2012a) on Hn 23, we have analyzed the *Gaia*-ESO spectrum of the Cha I member #36 by adopting the same procedure and tools (linelist, atmospheric models, etc.) used by Biazzo et al. (2012a). The derived atmospheric parameters, $T_{\rm eff}$ = 5230 ± 40 K, log g = 3.95 ± 0.15 dex and [Fe/H] = −0.08 ± 0.07 dex, are in excellent agreement with those produced by the *Gaia*-ESO Survey.

5.3. Metallicity in nearby YOCs and SFRs

Recently, Biazzo et al. (2011a) have presented a comprehensive comparison of the metallicity of YOCs and SFRs in the solar neighborhood (within 500 pc from the Sun). They showed that YOCs have an iron content similar to the solar value, while SFRs appear slightly more metal-poor than the Sun. In particular and most interestingly, no metal-rich SFRs seem to exist within this volume. However, these conclusions are based both on small number statistics (typically, 1−5 stars per region), and on [Fe/H] values that are determined from different observations and methods of analysis. Therefore, new homogeneous studies are needed to enable a more rigorous view on the metal content in nearby YOCs and SFRs to be developed. The *Gaia*-ESO Survey will contribute significantly to this aspect.

Our metallicity determination of Cha I, the first SFR observed by the *Gaia*-ESO Survey, is in line with other metal-poor SFRs analyzed by Biazzo et al. (2011a). Similarly, Gamma Velorum, the first YOC of the *Gaia*-ESO Survey, with an iron content of ⟨[Fe/H]⟩ = −0.057 ± 0.018 dex (Spina et al. 2014) is consistent with Cha I within the errors. We have also shown that there is no dependence of [Fe/H] on effective temperature in both cases. Hence, the two regions share the same metallicity and, most importantly, the determination is based on the same methods. Although definitive conclusions will be drawn once the *Gaia*-ESO consortium will produce the analysis of additional regions, the initial evidence suggests that: i) there is no systematic offset between the metallicity of YOCs and SFRs due to the analysis; ii) young clusters can also be more metal poor than the Sun, implying that their subsolar abundance is possibly related to their origin.

To further investigate this aspect, we display in Fig. 10 the metallicity distribution of all the clusters in the solar neighborhood with a determination of the iron abundance based on spectra characterized by a S/N greater than 20 and a resolution greater than R ∼ 7500. These determinations are listed in Table 1. The clusters cover a range in [Fe/H] from −0.20 to +0.27 dex, but the youngest associations (≲100 Myr) are generally restricted to the low metallicity values. Because of their young ages, these regions have not had time to migrate through and disperse in the Galactic disk. Thus, their metal content is representative of the present chemical pattern of the interstellar medium in the solar neighborhood. Since the chemical content and metallicity provide a powerful tool for tagging groups of stars or associations to a common formation site (Freeman & Bland-Hawthorn 2002; Tabernero et al. 2012; Mitschang et al. 2013; Magrini et al. 2014), the result of Fig. 10 suggests these young associations may share the same origin.

In this context, it is interesting to consider the Gould Belt (GB), a structure clearly visible in the sky as a large ring of mainly O- and B-type stars (for a detailed discussion see Poppel 1997). The ring has a diameter of ∼1000 pc and is tilted by ∼20° with respect to the Galactic plane. The GB is a relatively recent structure that formed between 20 and 90 Myr ago (Torra et al. 2000). Currently, the Sun is located within the ring at ∼100 pc from its center. The origin of the GB is still uncertain. Some studies suggest that the structure formed from the strong stellar wind originating in the central Cas-Tau OB association (e.g., Blaauw 1991; Poppel 1997, and references therein). Other authors proposed that the GB formed from the collision of high-velocity clouds with the interstellar medium of the Galactic disk (e.g., Comeron & Torra 1994). However, a combined scenario is also conceivable: the stellar feedback of massive OB stars and supernovae compressed the medium in the Galactic disk generating an expanding gaseous ring and simultaneously blowing out clumps of gas that subsequently fell back into the mid-plane of the galactic disk (Bally 2008).

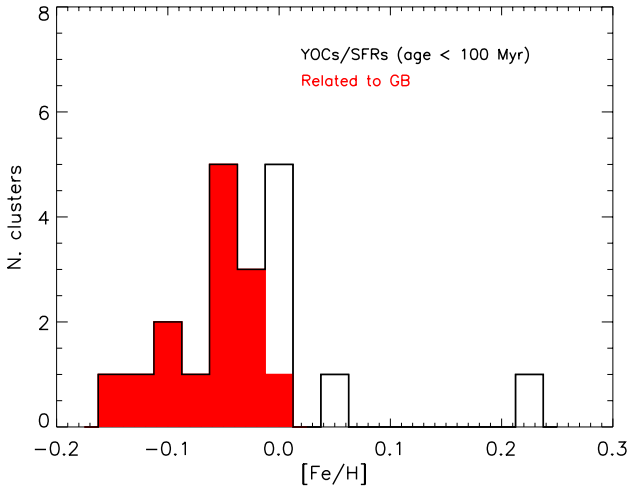

Fig. 11. Iron abundance distribution of the YOCs/SFRs in the solar neighborhood. The colored part of the histogram indicates the objects associated with the GB.

Remarkably, the GB contains most of the SFRs and YOCs in the solar neighborhood: in the last column of Table 1, we report the information on whether or not the cluster is associated with the GB according to the studies by Poppel (1997); de Zeeuw et al. (1999); Elias et al. (2009). For the latter study, we consider those clusters with a probability greater than 90% as associated with the GB. In Fig. 11, we plot the metallicity distribution of the clusters with an age $\leq$ 100 Myr, separately for clusters associated and not associated with the GB. The figure and the table clearly show that a large fraction of the nearby clusters are indeed associated with the GB and that most of them have subsolar metallicity. Conversely, the most metal-rich clusters and SFRs in the sample are not associated with the GB. We performed a two sample test using the ASURV survival analysis package (Lavalley et al. 1992) and found that the probability that clusters associated and not associated with the GB are drawn from the same parent population is below 0.3%, or, conversely, these two distributions of metallicity are different at the 3σ level. These facts lead us to suggest that the SFRs and YOCs associated with the GB show a metallicity distinctively lower than that of the Sun and that this could offer a reasonable explanation for the metal-poor nature found for most of the youngest stars in the solar neighborhood.

We caution that this conclusion is tentative due to the small sample analyzed so far. For example, one might argue that metal-rich clusters related to the GB do exist but have not yet been observed due to the still low number statistics. We also have already pointed out that most of the metallicity determinations are heterogeneous and, in some cases, affected by large errors. Furthermore, uncertainties in distances and proper motions prevent a conclusive assessment of the association of the various SFRs and YOCs with the GB. Hence, additional homogeneous and accurate information on the chemistry, the kinematics, and the dynamics is needed to further investigate the issue. The *Gaia*-ESO Survey will soon provide critical data on several other young clusters. Similarly, the *Gaia* mission will trace the GB structure with unprecedented accuracy, removing the uncertainty on membership and dynamical history. If these critical measurements confirm the metal-poor nature of the clusters/SFRs associated with the GB, it will certainly give important hints on the processes that generated the GB itself.

6. Conclusions

In this paper, we have used the dataset provided by the *Gaia*-ESO Survey to confirm the membership of Cha I of a number of the candidate members identified by L08 and to study their metallicities. We have found that Cha I has a slightly subsolar iron abundance, $\langle$[Fe/H]$\rangle$ = −0.08 ± 0.04 dex, derived from nine members observed with UVES and located in different parts of the complex. The small dispersion suggests that the two stellar groups of Cha I and the sparse population have a homogeneous metal content, as expected for a T Tauri association, such as Cha I that is isolated from other SFRs, YOCs, and OB associations.

The other findings can be summarized as follows:

i) We have confirmed the membership of Cha I of fifteen L08 stars on the basis of the surface gravity, the presence of photospheric lithium, and their position in the HRD. These stars belong to the two sub-clusters Cha I North and South and to the sparse population around the main molecular cloud. The sample of UVES targets does not contain any new member of Cha I.

ii) Our determination of the metallicity allows us to better constrain the [Fe/H] distribution and the average [Fe/H] value of Cha I. The mean value of [Fe/H] agrees reasonably well with that obtained by Padgett (1996), but our dispersion is much smaller. The metallicity of Cha I is also similar to that of Cha II derived by Biazzo et al. (2012a). This result indicates that the whole Chamaeleon complex is more metal-poor than the Sun.

iii) We speculate that the metallicity of Cha I is similar to that of other SFRs in the solar neighborhood. The metal-poor nature of these young environments could be the result of a common and widespread star formation episode that involved the Gould Belt and that gave birth to most of the SFRs and YOCs in the solar vicinity.

Our study not only reinforces the hints that the youngest stars in the Solar neighborhood are poorer in metals than the Sun itself but also shows the great potential of the *Gaia*-ESO Survey on this type of scientific research thanks to its homogeneous analysis and the rich statistics.

Acknowledgements. Based on data products from observations made with ESO Telescopes at the La Silla Paranal Observatory under programme ID 188.B-3002. This work was partly supported by the European Union FP7 programme through ERC grant number 320360 and by the Leverhulme Trust through grant RPG-2012-541. We acknowledge the support from INAF and Ministero dell' Istruzione, dell' Università' e della Ricerca (MIUR) in the form of the grant "Premiale VLT 2012". The results presented here benefit from discussions held during the *Gaia*-ESO workshops and conferences supported by the ESF (European Science Foundation) through the GREAT Research Network Programme. We acknowledge the use of the ASURV astronomy survival analysis package (Lavalley et al. 1992) which is freely available from `http://www.astro.psu.edu/statcodes/asurv`. E.D.M., S.G.S. and V.Zh.A. acknowledge the support from the Fundação para a Ciência e Tecnologia, FCT (Portugal) in the form of the fellowships SFRH/BPD/76606/2011, SFRH/BPD/47611/2008 and SFRH/BPD/70574/2010 from the FCT (Portugal), respectively. We also acknowledge the support of the French Agence Nationale de la Recherche, under contract ANR-2010-BLAN-0508-01OTP, and the "Programme National de Cosmologie et Galaxies" (PNCG) of CNRS/INSU, France. J.I.G.H. acknowledges financial support from the Spanish Ministry project MINECO AYA2011-29060, and also from the Spanish Ministry of Economy and Competitiveness (MINECO) under the 2011 Severo Ochoa Program MINECO SEV-2011-0187. H.M.T. and D.M. acknowledges financial support from the Spanish Ministry of Economy and Competitiveness (MINECO) project AYA2011-30147-C03-02. T.B. was funded by grant No. 621-2009-3911 from The Swedish Research Council.

References

Adibekyan, V. Z., Delgado Mena, E., Sousa, S. G., et al. 2012a, A&A, 547, A36
Adibekyan, V. Z., Santos, N. C., Sousa, S. G., et al. 2012b, A&A, 543, A89
Bally, J. 2008, Overview of the Orion Complex, ed. B. Reipurth, 459
Barrado y Navascués, D., Stauffer, J. R., & Patten, B. M. 1999, ApJ, 522, L53
Barrado y Navascués, D., Stauffer, J. R., & Jayawardhana, R. 2004, ApJ, 614, 386
Biazzo, K., Randich, S., & Palla, F. 2011a, A&A, 525, A35
Biazzo, K., Randich, S., Palla, F., & Briceño, C. 2011b, A&A, 530, A19
Biazzo, K., Alcalá, J. M., Covino, E., et al. 2012a, A&A, 547, A104
Biazzo, K., D'Orazi, V., Desidera, S., et al. 2012b, MNRAS, 427, 2905
Blaauw, A. 1991, in The Physics of Star Formation and Early Stellar Evolution, eds. C. J. Lada, & N. D. Kylafis, NATO ASIC Proc. 342, 125
Briceño, C., Calvet, N., Kenyon, S., & Hartmann, L. 1999, AJ, 118, 1354
Briceño, C., Calvet, N., Hernández, J., et al. 2005, AJ, 129, 907
Briceño, C., Hartmann, L., Hernández, J., et al. 2007, ApJ, 661, 1119
Brown, A. G. A., de Geus, E. J., & de Zeeuw, P. T. 1994, A&A, 289, 101
Cambresy, L. 1998, in The Impact of Near-Infrared Sky Surveys on Galactic and Extragalactic Astronomy, ed. N. Epchtein, Astrophys. Space Sci. Lib., 230, 157
Carraro, G., de La Fuente Marcos, R., Villanova, S., et al. 2007, A&A, 466, 931
Carrera, R., & Pancino, E. 2011, A&A, 535, A30
Casewell, S. L., Jameson, R. F., & Dobbie, P. D. 2006, MNRAS, 365, 447
Clem, J. L., Landolt, A. U., Hoard, D. W., & Wachter, S. 2011, AJ, 141, 115
Comerón, F. 2008, The Lupus Clouds, ed. B. Reipurth, 295
Comeron, F., & Torra, J. 1994, A&A, 281, 35
Covino, E., Alcala, J. M., Allain, S., et al. 1997, A&A, 328, 187
Cutri, R. M., Skrutskie, M. F., van Dyk, S., et al. 2003, 2MASS All Sky Catalog of point sources
de Geus, E. J., de Zeeuw, P. T., & Lub, J. 1989, A&A, 216, 44
de Zeeuw, P. T., Hoogerwerf, R., de Bruijne, J. H. J., Brown, A. G. A., & Blaauw, A. 1999, AJ, 117, 354
Dias, W. S., Alessi, B. S., Moitinho, A., & Lépine, J. R. D. 2002, A&A, 389, 871
Dolan, C. J., & Mathieu, R. D. 2002, AJ, 123, 387
D'Orazi, V., & Randich, S. 2009, A&A, 501, 553
D'Orazi, V., Randich, S., Flaccomio, E., et al. 2009, A&A, 501, 973
D'Orazi, V., Biazzo, K., & Randich, S. 2011, A&A, 526, A103
Elias, F., Alfaro, E. J., & Cabrera-Caño, J. 2009, MNRAS, 397, 2
Ercolano, B., & Clarke, C. J. 2010, MNRAS, 402, 2735
Ford, A., Jeffries, R. D., & Smalley, B. 2005, MNRAS, 364, 272
Freeman, K., & Bland-Hawthorn, J. 2002, ARA&A, 40, 487
Gebran, M., Monier, R., & Richard, O. 2008, Contributions of the Astronomical Observatory Skalnate Pleso, 38, 405
Gilli, G., Israelian, G., Ecuvillon, A., Santos, N. C., & Mayor, M. 2006, A&A, 449, 723
Gilmore, G., Randich, S., Asplund, M., et al. 2012, The Messenger, 147, 25
Gonzalez, G., & Lambert, D. L. 1996, AJ, 111, 424
González Hernández, J. I., Caballero, J. A., Rebolo, R., et al. 2008, A&A, 490, 1135
Grevesse, N., Asplund, M., & Sauval, A. J. 2007, Space Sci. Rev., 130, 105
Gustafsson, B., Edvardsson, B., Eriksson, K., et al. 2008, A&A, 486, 951
Hoogerwerf, R., & Blaauw, A. 2000, A&A, 360, 391
Hughes, J., Hartigan, P., Krautter, J., & Kelemen, J. 1994, AJ, 108, 1071
Hünsch, M., Randich, S., Weidner, C., Hempel, M., & Schmitt, J. H. M. M. 2004, in Stars as Suns: Activity, Evolution and Planets, eds. A. K. Dupree, & A. O. Benz, IAU Symp., 219, 980
James, D. J., Melo, C., Santos, N. C., & Bouvier, J. 2006, A&A, 446, 971
Jeffries, R. D., Totten, E. J., Harmer, S., & Deliyannis, C. P. 2002, MNRAS, 336, 1109
Jeffries, R. D., Naylor, T., Walter, F. M., Pozzo, M. P., & Devey, C. R. 2009, MNRAS, 393, 538
Jeffries, R. D., Jackson, R., Cottaar, M., Kosopov, A., et al. 2014, A&A, 563, A94
Jones, B. F., & Prosser, C. F. 1996, AJ, 111, 1193
Jones, B. F., Shetrone, M., Fischer, D., & Soderblom, D. R. 1996, AJ, 112, 186
Kang, W., Lee, S.-G., & Kim, K.-M. 2011, ApJ, 736, 87
Kharchenko, N. V., Piskunov, A. E., Röser, S., Schilbach, E., & Scholz, R.-D. 2005, A&A, 438, 1163
Lafrenière, D., Jayawardhana, R., Brandeker, A., Ahmic, M., & van Kerkwijk, M. H. 2008, ApJ, 683, 844
Lavalley, M., Isobe, T., & Feigelson, E. 1992, in Astronomical Data Analysis Software and Systems I, eds. D. M. Worrall, C. Biemesderfer, & J. Barnes, ASP Conf. Ser., 25, 245
Lombardi, M., Lada, C. J., & Alves, J. 2008, A&A, 480, 785
López Martí, B., Jiménez-Esteban, F., Bayo, A., et al. 2013, A&A, 556, A144
Luhman, K. L. 2007, ApJS, 173, 104
Luhman, K. L. 2008, Chamaeleon, ed. B. Reipurth, 169
Magrini, L., Randich, S., Romano, D., et al. 2014, A&A, 563, A44
Manzi, S., Randich, S., de Wit, W. J., & Palla, F. 2008, A&A, 479, 141
Menten, K. M., Reid, M. J., Forbrich, J., & Brunthaler, A. 2007, A&A, 474, 515
Mitschang, A. W., De Silva, G., Sharma, S., & Zucker, D. B. 2013, MNRAS, 428, 2321
Monet, A. K. B., Harris, H. C., & Hilton, J. 2008, in AAS/Division of Dynamical Astronomy Meeting, #39, #15.11
Neves, V., Santos, N. C., Sousa, S. G., Correia, A. C. M., & Israelian, G. 2009, A&A, 497, 563
Pace, G., Melendez, J., Pasquini, L., et al. 2009, A&A, 499, L9
Pace, G., Danziger, J., Carraro, G., et al. 2010, A&A, 515, A28
Padgett, D. L. 1996, ApJ, 471, 847
Panagi, P. M., & O'dell, M. A. 1997, A&AS, 121, 213
Pasquini, L., Avila, G., Blecha, A., et al. 2002, The Messenger, 110, 1
Pecaut, M. J., & Mamajek, E. E. 2013, ApJS, 208, 9
Pecaut, M. J., Mamajek, E. E., & Bubar, E. J. 2012, ApJ, 746, 154
Perryman, M. A. C., Brown, A. G. A., Lebreton, Y., et al. 1997, VizieR Online Data Catalog: J/A+A/331/81
Poppel, W. 1997, Fund. Cosmic Phys., 18, 1
Preibisch, T., & Mamajek, E. 2008, The Nearest OB Association: Scorpius-Centaurus (Sco OB2), ed. B. Reipurth, 235
Randich, S., & Gilmore, G. 2013, The Messenger, 154, 47
Robberto, M., Spina, L., Da Rio, N., et al. 2012, AJ, 144, 83
Robichon, N., Arenou, F., Mermilliod, J.-C., & Turon, C. 1999, A&A, 345, 471
Sacco, G. G., Morbidelli, L., Franciosini, E., et al. 2014, A&A, 565, A113
Salaris, M., Weiss, A., & Percival, S. M. 2004, A&A, 414, 163
Santos, N. C., Melo, C., James, D. J., et al. 2008, A&A, 480, 889
Santos, N. C., Lovis, C., Pace, G., Melendez, J., & Naef, D. 2009, A&A, 493, 309
Schuler, S. C., King, J. R., Fischer, D. A., Soderblom, D. R., & Jones, B. F. 2003, AJ, 125, 2085
Schwartz, R. D. 1977, ApJS, 35, 161
Sestito, P., Randich, S., Mermilliod, J.-C., & Pallavicini, R. 2003, A&A, 407, 289
Sestito, P., Randich, S., & Pallavicini, R. 2004, Mem. Soc. Astron. It., 75, 24
Shen, Z.-X., Jones, B., Lin, D. N. C., Liu, X.-W., & Li, S.-L. 2005, ApJ, 635, 608
Sherry, W. H., Walter, F. M., & Wolk, S. J. 2004, AJ, 128, 2316
Sicilia-Aguilar, A., Henning, T., Kainulainen, J., & Roccatagliata, V. 2011, ApJ, 736, 137
Siess, L., Dufour, E., & Forestini, M. 2000, A&A, 358, 593
Smiljanic, R., Gauderon, R., North, P., et al. 2009, A&A, 502, 267
Soderblom, D. R., Jones, B. F., Balachandran, S., et al. 1993, AJ, 106, 1059
Soderblom, D. R., Laskar, T., Valenti, J. A., Stauffer, J. R., & Rebull, L. M. 2009, AJ, 138, 1292
Spezzi, L., Alcalá, J. M., Covino, E., et al. 2008, ApJ, 680, 1295
Spezzi, L., de Marchi, G., Panagia, N., Sicilia-Aguilar, A., & Ercolano, B. 2012, MNRAS, 421, 78
Spina, L., Randich, S., Palla, F., et al. 2014, A&A, 567, A55
Stauffer, J. R., Hartmann, L. W., Prosser, C. F., et al. 1997, ApJ, 479, 776
Stauffer, J. R., Schild, R., Barrado y Navascues, D., et al. 1998, ApJ, 504, 805
Sung, H., Bessell, M. S., Lee, B.-W., & Lee, S.-G. 2002, AJ, 123, 290
Tabernero, H. M., Montes, D., & González Hernández, J. I. 2012, A&A, 547, A13
Terndrup, D. M., Pinsonneault, M., Jeffries, R. D., et al. 2002, ApJ, 576, 950
Torra, J., Fernández, D., & Figueras, F. 2000, A&A, 359, 82
van Leeuwen, F. 1999, in Harmonizing Cosmic Distance Scales in a Post-Hipparcos Era, eds. D. Egret, & A. Heck, ASP Conf. Ser., 167, 52
van Leeuwen, F. 2009, A&A, 497, 209
Viana Almeida, P., Santos, N. C., Melo, C., et al. 2009, A&A, 501, 965
Villanova, S., Carraro, G., & Saviane, I. 2009, A&A, 504, 845
Whittet, D. C. B., Prusti, T., Franco, G. A. P., et al. 1997, A&A, 327, 1194
Wichmann, R., Bastian, U., Krautter, J., Jankovics, I., & Rucinski, S. M. 1998, MNRAS, 301, L39
Wilking, B. A., Meyer, M. R., Robinson, J. G., & Greene, T. P. 2005, AJ, 130, 1733
Yasui, C., Kobayashi, N., Tokunaga, A. T., Saito, M., & Tokoku, C. 2010, ApJ, 723, L113
Zuckerman, B., Melis, C., Rhee, J. H., Schneider, A., & Song, I. 2012, ApJ, 752, 58

Pages 10 to 12 are available in the electronic edition of the journal at http://www.aanda.org

Table 1. Metallicity of open clusters in the solar neighborhood ($\lesssim$500 pc).

Name	Age (Myr)	Dist. (pc)	Ref.	[Fe/H] (dex)	# stars	Ref.	Gould Belt association
			Star-Forming Regions				
ONC	2	400	31	−0.11 ± 0.08	11	Biazzo et al. (2011a)	Y
Corona Australis	3	138	46	−0.06 ± 0.05	3	Santos et al. (2008)	Y
Lupus	3	155	3, 32	−0.05 ± 0.01	5	Santos et al. (2008)	Y
Rho Ophiuchi	3	120	26, 33	−0.14 ± 0.02	2	Randich et al. (2014)	Y
Taurus	1	140	12, 10	−0.01 ± 0.05	6	D'Orazi et al. (2011)	N
Cha I	2	160	30, 8	−0.08 ± 0.04	9	This work	Y
Cha II	4	178	36, 8	−0.12	1	Biazzo et al. (2012a)	Y
			Young Open Clusters				
Orion OB1b	5	400	28	−0.05 ± 0.05	5	Biazzo et al. (2011a)	Y
25 Ori	10	330	24	−0.05 ± 0.05	5	Biazzo et al. (2011b)	Y
Sigma Ori	4	360	23, 2	−0.02 ± 0.09	9	González Hernández et al. (2008)	Y
Lambda Ori	10	400	17	0.01 ± 0.01	5	Biazzo et al. (2011b)	Y
Gamma Velorum	10	350	37	−0.057 ± 0.018	7	Spina et al. (2014)	Y
IC 2602	30	145	15, 7	0.00 ± 0.01	8	D'Orazi & Randich (2009)	N
IC 2391	55	149	15, 11, 21	−0.01 ± 0.02	7	D'Orazi & Randich (2009)	N
IC 4665	25	385	34, 16	−0.03 ± 0.04	18	Shen et al. (2005)	Y
NGC 2451A	57	188	25, 14	−0.01 ± 0.08	6	Hünsch et al. (2004)	N
Melotte 20	60	172	46, 40	0.23 ± 0.08	2	Gonzalez & Lambert (1996)	N
Blanco 1	90	207	5, 40	0.04 ± 0.02	8	Ford et al. (2005)	N
Upper Scorpius	10	140	45, 35	−0.09 ± 0.10	6	Randich et al. (2014)	Y
Upper Centaurus Lupus	16	140	1, 13	−0.02 ± 0.05	2	Randich et al. (2014)	Y
			Older Open Clusters				
Hyades	625	46	6	0.11 ± 0.01	3	Carrera & Pancino (2011)	N
IC 4756	790	430	22, 41	0.02 ± 0.03	6	Santos et al. (2009)	N
M34	200–250	475	4	0.07 ± 0.04	9	Schuler et al. (2003)	N
Melotte 111	450	86	27, 15	0.06 ± 0.10	22	Gebran et al. (2008)	N
NGC 752	1590	400	42	0.01 ± 0.04	18	Sestito et al. (2004)	N
NGC 1901	400	400	29	−0.08	1	Carraro et al. (2007)	N
NGC 2516	158	360	20	0.01 ± 0.07	2	Terndrup et al. (2002)	N
NGC 3532	320	492	43	0.04 ± 0.05	6	Smiljanic et al. (2009)	N
NGC 6281	316	512	38	0.05 ± 0.06	2	Smiljanic et al. (2009)	N
NGC 6475	200	300	39	0.14 ± 0.06	13	Sestito et al. (2003)	N
NGC 6633	600	376	18, 19	0.06 ± 0.01	3	Santos et al. (2009)	N
Pleiades	120	120	9, 40	0.07 ± 0.05	20	Soderblom et al. (2009)	N
Praesepe	794	182	25, 40	0.27 ± 0.04	7	Pace et al. (2009)	N

References. 1: de Geus et al. (1989); 2: Brown et al. (1994); 3: Hughes et al. (1994); 4: Jones & Prosser (1996); 5: Panagi & O'dell (1997); 6: Perryman et al. (1997); 7: Stauffer et al. (1997); 8: Whittet et al. (1997); 9: Stauffer et al. (1998); 10: Wichmann et al. (1998); 11: Barrado y Navascués et al. (1999); 12: Briceño et al. (1999); 13: de Zeeuw et al. (1999); 14: Robichon et al. (1999); 15: van Leeuwen (1999); 16: Hoogerwerf & Blaauw (2000); 17: Dolan & Mathieu (2002); 18: Dias et al. (2002); 19: Jeffries et al. (2002); 20: Sung et al. (2002); 21: Barrado y Navascués et al. (2004); 22: Salaris et al. (2004); 23: Sherry et al. (2004); 24: Briceño et al. (2005); 25: Kharchenko et al. (2005); 26: Wilking et al. (2005); 27: Casewell et al. (2006); 28: Briceño et al. (2007); 29: Carraro et al. (2007); 30: Luhman (2007); 31: Menten et al. (2007); 32: Comerón (2008); 33: Lombardi et al. (2008); 34: Manzi et al. (2008); 35: Preibisch & Mamajek (2008); 36: Spezzi et al. (2008); 37: Jeffries et al. (2009); 38: Smiljanic et al. (2009); 39: Villanova et al. (2009); 40: van Leeuwen (2009); 41: Pace et al. (2010); 42: Carrera & Pancino (2011); 43: Clem et al. (2011); 44: Sicilia-Aguilar et al. (2011); 45: Pecaut et al. (2012); 46: Zuckerman et al. (2012).

Table 2. Target stars.

ID	CNAME	RA (J2000)	Dec (J2000)	J_{2MASS} (mag)	S/N	Membership (L08)	Tight system*
1	10554858-7651504	10 55 48.58	−76 51 50.4	9.58	103	–	–
2	10555973-7724399	10 55 59.73	−77 24 39.9	10.78	6	Y	N
3	10564115-7744292	10 56 41.15	−77 44 29.2	7.72	74	–	–
4	10574797-7617429	10 57 47.97	−76 17 42.9	7.84	101	–	–
5	10585418-7743115	10 58 54.18	−77 43 11.5	10.79	48	–	–
6	10590108-7722407	10 59 01.08	−77 22 40.7	10.14	26	Y	N
7	10593816-7822421	10 59 38.16	−78 22 42.1	7.74	73	–	–
8	11010007-7738516	11 01 00.07	−77 38 51.6	9.49	45	–	–
9	11012887-7539520	11 01 28.87	−75 39 52.0	7.02	274	–	–
10	11020524-7525093	11 02 05.24	−75 25 09.3	7.27	99	–	–
11	11022491-7733357	11 02 24.91	−77 33 35.7	9.10	77	Y	N
12	11033599-7628242	11 03 35.99	−76 28 24.2	8.71	62	–	–
13	11034945-7700101	11 03 49.45	−77 00 10.1	8.58	22	–	–
14	11044460-7706240	11 04 44.60	−77 06 24.0	9.60	34	–	–
15	11045100-7625240	11 04 51.00	−76 25 24.0	10.54	27	Y	N
16	11053303-7700120	11 05 33.03	−77 00 12.0	10.73	12	–	–
17	11055780-7607489	11 05 57.80	−76 07 48.9	7.15	296	Y	N
18	11060511-7511454	11 06 05.11	−75 11 45.4	7.72	129	–	–
19	11064510-7727023	11 06 45.10	−77 27 02.3	10.18	9	Y	N
20	11065856-7713326	11 06 58.56	−77 13 32.6	7.70	47	–	–
21	11075588-7727257	11 07 55.88	−77 27 25.7	9.22	38	Y	Y
22	11080148-7742288	11 08 01.48	−77 42 28.8	8.70	80	Y	Y
23	11080412-7513273	11 08 04.12	−75 13 27.3	8.92	65	–	–
24	11082577-7648315	11 08 25.77	−76 48 31.5	7.88	86	–	–
25	11084041-7756310	11 08 40.41	−77 56 31.0	9.90	69	–	–
26	11085231-7743329	11 08 52.31	−77 43 32.9	12.85	<5	–	–
27	11085326-7519374	11 08 53.26	−75 19 37.4	9.74	42	Y	–
28	11091172-7729124	11 09 11.72	−77 29 12.4	9.93	39	Y	Y
29	11091769-7627578	11 09 17.69	−76 27 57.8	10.00	58	Y	Y
30	11092378-7623207	11 09 23.78	−76 23 20.7	10.44	93	Y	N
31	11095119-7658568	11 09 51.19	−76 58 56.8	9.52	47	–	–
32	11100704-7629377	11 10 07.04	−76 29 37.7	9.91	59	Y	Y
33	11111333-7731178	11 11 13.33	−77 31 17.8	8.02	42	–	–
34	11112801-7749213	11 11 28.01	−77 49 21.3	8.77	56	–	–
35	11114632-7620092	11 11 46.32	−76 20 09.2	9.11	147	Y	N
36	11124268-7722230	11 12 42.68	−77 22 23.0	8.65	169	Y	Y
37	11124299-7637049	11 12 42.99	−76 37 04.9	10.06	92	Y	N
38	11135757-7818460	11 13 57.57	−78 18 46.0	14.93	<5	–	–
39	11140585-7729058	11 14 05.85	−77 29 05.8	8.31	45	–	–
40	11140941-7714492	11 14 09.41	−77 14 49.2	7.37	121	–	–
41	11141568-7738326	11 14 15.68	−77 38 32.6	10.72	58	–	–
42	11142964-7707063	11 14 29.64	−77 07 06.3	9.69	64	–	–
43	11143515-7539288	11 14 35.15	−75 39 28.8	9.29	84	–	–
44	11170509-7538518	11 17 05.09	−75 38 51.8	7.35	137	–	–
45	11182024-7621576	11 18 20.24	−76 21 57.6	9.79	40	Y	Y
46	11213017-7616098	11 21 30.17	−76 16 09.8	9.59	65	–	–
47	11252677-7553273	11 25 26.77	−75 53 27.3	8.50	127	–	–
48	11291261-7546263	11 29 12.61	−75 46 26.3	9.82	38	Y	–

Notes. (*) We consider "tight systems" only the multiple systems with a separation ≤2″ between the components, assuming the determinations from Lafrenière et al. (2008).

Table 3. Stellar parameters of the 48 UVES stars.

ID	RV ($km\,s^{-1}$)	$v \sin i$ ($km\,s^{-1}$)	$T_{\rm eff}$ (K)	log g (dex)	[Fe/H] (dex)	EW(Li) mÅ	$L_{\rm bol}$ ($L_\odot$)	bin.	log g mem.	Li mem.	HRD mem.	Final mem.
1	44.0 ± 0.6	...	...	...	...	<15	...	N	–	–	–	–
2	...	...	3640 ± 300	4.40 ± 0.20	−0.10 ± 0.20	406 ± 51	$0.38^{+0.15}_{-0.09}$	N	Y	Y	Y	Y
3	−1.9 ± 0.6	0.8 ± 0.9	4384 ± 51	2.02 ± 0.18	−0.33 ± 0.08	104 ± 1	...	N	N	–	–	N
4	4.8 ± 0.6	2.1 ± 1.4	5110 ± 49	3.08 ± 0.16	0.19 ± 0.12	15 ± 10	...	N	N	–	–	N
5	10.4 ± 0.6	0.5 ± 0.5	4701 ± 60	2.99 ± 0.17	0.13 ± 0.10	<15	...	N	N	–	–	N
6	15.3 ± 0.6	8.8 ± 0.8	4135 ± 125	4.63 ± 0.13	−0.09 ± 0.13	569 ± 18	$0.79^{+0.26}_{-0.19}$	N	Y	Y	Y	Y
7	10.0 ± 0.6	0.5 ± 0.5	4464 ± 55	2.25 ± 0.20	−0.09 ± 0.12	<10	...	N	N	–	–	N
8	108.1 ± 0.2	2.1 ± 1.9	3958 ± 63	1.85 ± 0.49	−0.31 ± 0.15	317 ± 5	...	N	N	–	–	N
9	...	...	...	...	...	<2	...	N	–	–	–	–
10	−28.1 ± 0.6	1.2 ± 1.5	4253 ± 67	1.77 ± 0.28	−0.23 ± 0.08	<5	...	N	N	–	–	N
11	14.2 ± 0.6	14.1 ± 1.2	4656 ± 193	4.28 ± 0.52	−0.16 ± 0.11	571 ± 5	$1.74^{+0.71}_{-0.53}$	N	Y	Y	Y	Y
12	11.9 ± 0.6	1.0 ± 1.2	4242 ± 80	1.85 ± 0.34	−0.22 ± 0.06	35 ± 2	...	N	N	–	–	N
13	−41.5 ± 0.6	0.5 ± 0.5	3865 ± 72	1.54 ± 0.12	0.03 ± 0.11	<30	...	N	N	–	–	N
14	28.9 ± 0.6	0.6 ± 0.6	4411 ± 60	1.99 ± 0.18	−0.30 ± 0.07	<10	...	N	N	–	–	N
15	13.5 ± 0.6	13.8 ± 1.2	4571 ± 333	4.44 ± 0.16	0.00 ± 0.16	575 ± 6	$0.50^{+0.29}_{-0.19}$	N	Y	Y	Y	Y
16	8.9 ± 0.6	2.2 ± 1.7	4631 ± 417	4.39 ± 0.35	−0.12 ± 0.12	30 ± 10	...	N	Y	N	–	N
17	...	...	...	...	...	<5	...	N	–	–	–	–
18	77.1 ± 0.6	3.2 ± 1.6	5003 ± 39	2.69 ± 0.16	−0.33 ± 0.17	<5	...	N	N	–	–	N
19	15.4 ± 0.6	19.3 ± 2.5	4343 ± 147	4.56 ± 0.15	−0.07 ± 0.13	797 ± 32	$1.10^{+0.40}_{-0.30}$	N	Y	Y	Y	Y
20	−8.6 ± 0.2	0.8 ± 1.0	3777 ± 85*	1.44 ± 0.20*	0.02 ± 0.11*	212 ± 45	...	N	N	–	–	N
21	17.5 ± 0.6	9.1 ± 1.4	4651 ± 174	4.10 ± 0.57	−0.25 ± 0.23	499 ± 3	$5.39^{+2.08}_{-1.59}$	N	Y	Y	Y	Y
22	4.5 ± 0.6	23.3 ± 4.6	4327 ± 131	4.44 ± 0.12	−0.10 ± 0.14	555 ± 13	...	Y	–	–	–	–
23	−15.6 ± 0.6	0.5 ± 0.6	4436 ± 91	2.15 ± 0.18	−0.11 ± 0.10	36 ± 9	...	N	N	–	–	N
24	15.9 ± 0.6	0.5 ± 0.5	4485 ± 53	2.22 ± 0.16	−0.01 ± 0.16	<5	...	N	N	–	–	N
25	−6.5 ± 0.6	29.9 ± 6.2	6378 ± 183	3.94 ± 0.17	−0.01 ± 0.12	97 ± 15	...	N	Y	HCM	N	N
26	...	...	...	...	...	<5	...	N	–	–	–	–
27	50.3 ± 0.6	...	...	...	...	428 ± 8	...	Y	–	–	–	–
28	14.8 ± 0.6	5.0 ± 1.6	4175 ± 381	4.38 ± 0.60	−0.45 ± 0.44	654 ± 15	$0.74^{+0.49}_{-0.25}$	N	Y	Y	Y	Y
29	15.1 ± 0.6	14.8 ± 1.2	4524 ± 103	4.21 ± 0.58	−0.14 ± 0.12	567 ± 10	$1.41^{+0.44}_{-0.35}$	N	Y	Y	Y	Y
30	...	...	3990 ± 123	4.64 ± 0.13	−0.09 ± 0.13	547 ± 15	$1.21^{+0.34}_{-0.28}$	N	Y	Y	Y	Y
31	35.1 ± 0.6	0.5 ± 0.5	5755 ± 76	4.28 ± 0.19	0.49 ± 0.15	<10	...	N	Y	N	–	N
32	14.0 ± 0.6	5.1 ± 1.2	4697 ± 120	4.37 ± 0.43	−0.32 ± 0.27	563 ± 6	$1.75^{+0.57}_{-0.46}$	N	Y	Y	Y	Y
33	21.6 ± 0.6	0.5 ± 0.5	4794 ± 43	3.15 ± 0.14	0.21 ± 0.16	<10	...	N	N	–	–	N
34	−28.2 ± 0.6	0.7 ± 0.8	3928 ± 118	1.43 ± 0.20	−0.11 ± 0.12	20 ± 10	...	N	N	–	–	N
35	16.2 ± 0.6	24.2 ± 1.4	4617 ± 207	4.50 ± 0.17	−0.06 ± 0.14	537 ± 15	$2.54^{+1.08}_{-0.80}$	N	Y	Y	Y	Y
36	14.2 ± 0.6	8.6 ± 0.8	5239 ± 70	4.23 ± 0.34	−0.08 ± 0.08	369 ± 4	$3.87^{+1.04}_{-0.86}$	N	Y	Y	Y	Y
37	14.3 ± 0.6	12.2 ± 0.9	4706 ± 220	4.27 ± 0.42	−0.06 ± 0.11	461 ± 5	$0.77^{+0.33}_{-0.25}$	N	Y	Y	Y	Y
38	...	...	...	...	...	<5	...	N	–	–	–	–
39	−3.7 ± 0.6	0.7 ± 0.8	3972 ± 103	1.55 ± 0.24	0.00 ± 0.10	<28	...	N	N	–	–	N
40	−24.5 ± 0.6	1.5 ± 1.7	4105 ± 65	1.59 ± 0.21	−0.29 ± 0.07	<10	...	N	N	–	–	N
41	14.8 ± 0.6	99.4 ± 10.5	7075 ± 102	4.16 ± 0.14	−0.09 ± 0.13	<50	...	N	Y	HCM	N	N
42	−17.0 ± 0.6	1.9 ± 1.6	5968 ± 59	4.32 ± 0.11	0.03 ± 0.04	23 ± 3	...	N	Y	N	–	N
43	−9.1 ± 0.6	0.8 ± 0.9	4469 ± 43	2.05 ± 0.17	−0.26 ± 0.08	<10	...	N	N	–	–	N
44	7.0 ± 0.6	0.5 ± 0.5	4882 ± 56	2.80 ± 0.15	0.08 ± 0.14	15 ± 5	...	N	N	–	–	N
45	13.8 ± 0.6	8.3 ± 1.2	4465 ± 209	4.25 ± 0.58	−0.19 ± 0.21	529 ± 7	$0.84^{+0.37}_{-0.26}$	N	Y	Y	Y	Y
46	−30.4 ± 0.6	1.0 ± 1.1	4917 ± 50	2.86 ± 0.12	0.05 ± 0.08	<10	...	N	N	–	–	N
47	−5.8 ± 0.6	19.0 ± 2.1	6380 ± 207	4.04 ± 0.22	−0.01 ± 0.15	<10	...	N	Y	N	–	N
48	15.2 ± 0.6	20.8 ± 1.2	4818 ± 96	4.50 ± 0.15	−0.06 ± 0.14	463 ± 7	$1.14^{+0.33}_{-0.28}$	N	Y	Y	Y	Y

Notes. (*) For object #20 the stellar parameters do not come from GESviDR1Final catalog, but they are only computed by one node.